Journal of Applied Physics

Van der Waals heterostructures of blue phosphorene and scandium-based MXenes monolayers

Cite as: J. Appl. Phys. **126**, 143101 (2019); https://doi.org/10.1063/1.5114850
Submitted: 12 June 2019 . Accepted: 17 September 2019 . Published Online: 08 October 2019

Gul Rehman, Shujaat Ali Khan, Roshan Ali, Iftikhar Ahmad, Li-Yong Gan, and Bin Amin

Journal of Applied Physics ARTICLE scitation.org/journal/jap

Van der Waals heterostructures of blue phosphorene and scandium-based MXenes monolayers

Cite as: J. Appl. Phys. **126**, 143101 (2019); doi: 10.1063/1.5114850
Submitted: 12 June 2019 · Accepted: 17 September 2019 ·
Published Online: 8 October 2019

Gul Rehman,[1,2] Shujaat Ali Khan,[3] Roshan Ali,[4] Iftikhar Ahmad,[2,5,a)] Li-Yong Gan,[6,a)] and Bin Amin[5,a)]

AFFILIATIONS

[1]Department of Physics, University of Malakand, Chakdara 18800, Pakistan
[2]Center for Computational Materials Science, University of Malakand, Chakdara 18800, Pakistan
[3]Department of Physics, Hazara University, Mansehra 21300, Pakistan
[4]The Guo China-US Photonics Laboratory, Changchun Institute of Optics, Fine Mechanics and Physics, Chinese Academy of Sciences, Changchun 130033, People's Republic of China
[5]Abbottabad University of Science and Technology, Abbottabad 22010, Pakistan
[6]Institute for Structure and Function and Department of Physics, Chongqing University, 400030 Chongqing, China

[a)]**Authors to whom correspondence should be addressed:** binukhn@gmail.com; ahma5532@gmail.com; and ganly@cqu.edu.cn

ABSTRACT

Stacked layers in the form of van der Waals (vdW) heterostructures can significantly extend the applications of its building materials. In this study, based on hybrid functional (HSE06) with vdW corrections, we systematically investigated the electronic structure and optical properties of BlueP/Sc_2CX_2 (X = O, F, OH) vdW heterostructures and their corresponding monolayers. All three heterostructures are indirect bandgap semiconductors with type-II band alignment. The calculated bandgap of BlueP/Sc_2CF_2 is found to be 1.528 eV. A small amount of charge transfers from BlueP to Sc_2CF_2 and from Sc_2CO_2 [$Sc_2C(OH)_2$] to BlueP, rendering it p- and n-doped, respectively. The formation of heterostructures enhanced the optical absorption in the visible light region as compared to their parent monolayer, particularly in BlueP/Sc_2CF_2 and BlueP/$Sc_2C(OH)_2$. Heterostructures show excellent device absorption efficiencies (70%–80%) from infrared to ultraviolet spectrum of light. These results suggest that BlueP/Sc_2CX_2 heterostructures are potential for nanoelectronics, optoelectronics, and photovoltaic device applications.

I. INTRODUCTION

Graphene[1] and monolayers of transition metal dichalcogenides (TMDCs),[2,3] hexagonal boron nitrides (h-BN),[4,5] metal oxides and hydroxides,[6] and black phosphorene (BlackP)[7] have created an unprecedented science sensation owing to their fascinating electronic, thermal, and mechanical properties. The unusual behaviors of two-dimensional (2D) materials, originating from quantum confinement, have shown many promising applications in nanoelectronics.[8–11] Therefore, researchers have paid significant attention to explorations of other 2D materials that have novel electronic and optoelectronic properties.

Recently, soon after the theoretical prediction of a new allotrope of bulk black phosphorus (BlackP),[7] named blue phosphorene (BlueP),[12] a single-layer BlueP has been fabricated by epitaxial growth on Au(111) and GaN(001) substrates.[13,14] BlueP is a semiconducting material with more symmetric buckled hexagonal structure than the puckered rectangular structure of BlackP and has been demonstrated to be equally stable as BlackP.[13] Unlike the semimetallic graphene, phosphorene has thickness-dependent bandgap ranging from 0.3 eV to 1.5 eV[15,16] and $\leq$3 eV[12] for BlackP and BlueP, respectively. Hence, they can cover spectral ranges from the visible to mid-infrared region, making them appealing for the nanoelectronic devices.[17] Moreover, phosphorene based transistors have shown high carrier mobilities (300–1000 $cm^2V^{-1}s^{-1}$) and high on/off ratios ($>10^5$).[18,19]

Among 2D material families, MXenes are synthesized by selectively etching **A** layers from bulk M**A**X phases,[20–23] where M

represents early transition elements, **A** is a group IIIA or IVA element, and X is carbon or nitrogen. In the etching process, bare MXenes are functionalized by O/F/OH functional groups on both surfaces.[24] MXenes have shown potentiality as catalysts,[25] spintronics,[26,27] Li/Na/K-ion batteries,[28–30] hybrid electrochemical capacitors,[31] and flexible devices.[32,33] Specifically, the monolayer Sc_2CO_2 is demonstrated to be most preferable for SO_2 molecule adsorption (as gas sensors or capturers).[34] Sc_2CT_2 (T = F and OH) MXenes exhibit good optical absorption in the visible light region, an efficient electron-hole separation, and high carrier mobility.[35]

The existing properties of 2D materials can be further tuned by doping/defects,[36] strain engineering,[37] alloying,[38] formation of heterojunctions and superlattices,[39,40] and applying an external electric field.[41] In these strategies, the heterojunctions combine together the advantageous properties of its building materials. Particularly, semiconducting 2D heterostructures play an important role in the development of modern electronic and optoelectronic devices and provide many new opportunities for achieving desired electronic and transport properties.[42–44] Vertical heterostructure is formed by stacking two different 2D material sheets on the top of each other via van der Waals (vdW) interactions and, hence, is called van der Waals heterostructures,[42] whereas lateral heterostructure is made from in-plane contacts between the sheets.

The vdW heterostructures have received increasing attention due to their unique properties such as a large interface area between the component materials, atomic-scale thickness, and, most importantly, the absence of dangling bonds.[45,46] Quantum coupling between stacked 2D layers causes new fascinating phenomena, hence leading to revolutionary optical/electronic devices, such as tunneling and bipolar transistors[42,43] and flexible optoelectronic devices.[44] For example, the photochemical performances and electronic conductivity are significantly improved in MoS_2/graphene heterostructures.[47,48] Specifically, type-II band alignment in the vdW heterostructure is useful for light detection and harvesting.[49,50] This type of band alignment facilitates efficient electron-hole separation and significantly reduces the charge recombination probability, thus highly desirable for photovoltaic and photocatalytic devices.[51,52]

Spontaneous charge separation in the WX_2/MoX_2 (X = S, Se, Te) heterojunction, when excitons diffuse through the junction, is appropriate for photovoltaics.[49] For example, the MoS_2/WSe_2 junction shows rapid photoresponse and remarkable current rectification with high quantum efficiency.[53] In the $MoSe_2/WSe_2$ heterostructure, long-lived interlayer excitons and indirect bandgap with type-II band alignment have been reported.[54] The BlackP/MoS_2 p-n diode demonstrates a photodetection responsivity of 418 mA/W, which is about 100 times higher than that of a black phosphorus phototransistor.[55] Employing density functional theory (DFT), WSe_2/Zr_2CO_2 and TMDCs/Sc_2CF_2 heterojunctions have been predicted to be type-II semiconductors.[56,57] Moderate in-plane strains were used to achieve a type-II semiconducting nature in the $MoSe_2/Zr_2CO_2$, SiC-MX_2 (M = Mo, W and X = S, Se), and MXene/MXene heterostructures.[56,58,59] Zr_2CO_2/BlueP heterostructure was found to be an indirect type-I semiconductor, while strains transform it into type-II alignment.[60] Peng *et al.* predicted 1.16% and 0.98% upper limit energy conversion efficiencies for BlueP/MoS_2 and BlueP/$MoSe_2$ heterostructures, respectively, signifying their potential applications in optoelectronic and efficient thin-film solar cells.[51] Using molecular dynamics simulations, thermal conductivity of phosphorene in phosphorene/graphene heterojunctions was investigated and found to be 20%–60% higher than the pristine one.[61] Accordingly, BlueP and Sc_2CX_2 (X = O, F, and OH) MXenes have high potential to generate interesting properties by creating heterostructures with each other.

In the present work, the electronic structures and optical properties of three vertical heterostructures, BlueP/Sc_2CO_2, BlueP/Sc_2CF_2, and BlueP/$Sc_2C(OH)_2$, are investigated. The vdW interaction is considered between the layers of the heterostructures. The stability of these systems is confirmed by means of calculating the binding energies and phonon spectra. All the systems retain their semiconducting nature and possesses type-II band alignment without any external effect (i.e., strain or electric field) that is highly desirable for photovoltaic devices.[62] Furthermore, heterostructures exhibit excellent optical absorption in the visible and ultraviolet regions. These findings of BlueP/Sc_2CX_2 (X = O, F, and OH) heterostructure will encourage experimentalists to realize the BlueP and MXenes nanocomposites in the near future.

II. COMPUTATIONAL DETAILS

DFT calculations were carried out using a projected augmented plane-wave (PAW) scheme as implemented in the Vienna ab initio simulation package (VASP) code[63–65] with generalized gradient approximation (GGA).[66] The semiempirical corrections approach of Grimme DFT-D2 was used for the vdW interaction between layers of heterostructure, while the semiclassical parameters C_6 and R_0 for all atoms were acquired from Table 1 of Ref. 67. The Γ-centered Monkhorst-Pack k-meshes of $6 \times 6 \times 1$ were used for the structural relaxation, which were refined to $12 \times 12 \times 1$ for the optimized structures. The plane wave cutoff was set to 550 eV. A convergence criterion of 10^{-4} eV/Å (10^{-5} eV) for force (energy) was adopted in geometry optimization (self-consistent calculations). A vacuum space of 20 Å was added along the z direction perpendicular to the 2D sheets for the elimination of the effect of spurious interaction between the adjacent layers.

Phonon spectrum calculation was carried out by phonopy code interfaced with the VASP, which uses the harmonic interatomic force constants (acquired by density functional perturbation theory). A $3 \times 3 \times 1$ supercell was used for these calculations.[68,69] In addition, as Perdew-Burke-Ernzerhof (PBE) functional underestimates the bandgap values of semiconductors, band structures of each monolayer and heterostructure were examined by the HSE06 hybrid functional.[70] The band edges of BlueP and MXenes were adjusted with respect to the vacuum energy level.

The optical absorption spectra were obtained by employing GW_0 approach, where single particle energies and wave functions obtained by HSE06 functional were used to calculate the quasiparticle energies and to solve the Bethe-Salpeter equation.[71,72] GW_0 calculations were performed by using an ENCUT of 420 eV, a k-mesh of $6 \times 6 \times 1$, and an NBAND of 300 and 10 highest/lowest valence/conduction bands for calculating the excitonic eigenstates. Different cutoffs and k-meshes were adopted due to the high computational cost of GW_0 calculations.

Absorption efficiencies were calculated by using the real $[\varepsilon_1(\omega)]$ and imaginary $[\varepsilon_2(\omega)]$ parts of the dielectric constants obtained from the GW_0 calculations as input files in the COMSOL

multiphysics simulation package. The same device was used as in Refs. 73 and 74 [see Fig. 6(e)]. In this device, a 100 nm thick layer of glass is used as the top layer. The second layer is indium doped tin oxide (ITO), which is 80 nm thick, and is used as the anode material. In this study, we have used a 350 nm thick 2D monolayer and heterostructure materials. Above the layer of the 2D material, we stacked a 10 nm thick PC60BM [(6,6)-phenyl-C61-butyric acid methyl ester] known as the electron transport layer (ETL), while below the 2D material layer, a 15 nm thick PCDTBT (poly(N-9 0-heptadecanyl-2,7-carbazole-alt-5,5-(4 0,7 0-di(thien-2-yl)-2 0,1 0,3 0-benzothiadiazole))) was used, which is known as a hole transport layer (HTL) for obtaining the excited carriers. The bottom cathode material consists of a 100 nm thick Ag layer.

III. RESULT AND DISCUSSION

Prior to comprehensive investigation of BlueP/Sc_2CX_2 heterostructures, we first examined the structural and electronic properties of individual BlueP and Sc_2CX_2 MXene monolayers. The hexagonal 2D structures of monolayers are presented in Fig. S1 of the supplementary material, and the optimized lattice parameters are tabulated in Table S1 of the supplementary material. In the phosphorene monolayer, each P atom is bonded with three neighboring P atoms, generating a buckled or puckered honeycomb structure akin to graphene. The unit cell of bare MXene (S_2C MXene) can be modeled as four types of hexagonal structures according to the adsorption positions of the functional O, OH, or F atoms on both sides of Sc_2C layers, which consists of a C layer sandwiched between two Sc layers (see Fig. 1 of Ref. 56). According to the position of the O, F, and OH terminations presented in Ref. 56, models 4 and 1 for Sc_2CO_2 and Sc_2CF_2 [$Sc_2C(OH)_2$] are energetically the most stable structure (see Fig. S1 in the supplementary material), respectively, and, hence, are used for further calculations. The lattice constants of BlueP, Sc_2CO_2, $Sc_2C(OH)_2$, and Sc_2CF_2 monolayers in our calculation are 3.29 Å, 3.407 Å, 3.25 Å, and 2.29 Å. Our optimized lattice parameters for BlueP and the most stable Sc_2CX_2 monolayers are consistent with the other reported values.[75,76]

The electronic band structures and projected density of states (PDOS) of the monolayers calculated by HSE06 are shown in Fig. S2 of the supplementary material . For comparison, band structures calculated with PBE functional are also presented. The HSE06 calculations show that the BlueP, Sc_2CO_2, and Sc_2CF_2 monolayers are indirect bandgap semiconductors with bandgaps of 2.833 eV, 2.820 eV, and 1.789 eV, respectively, whereas the $Sc_2C(OH)_2$ monolayer has a direct bandgap (0.7965 eV), and its valence band maximum (VBM) and the conduction band minimum (CBM) both reside at the Γ-point of the Brillouin zone (BZ). The VBM (CBM) of the BlueP, Sc_2CO_2, and Sc_2CF_2 monolayer are located along the M-Γ (M-Γ) direction, at the Γ (K)-point, and Γ (M) of point of BZ, respectively. For all these monolayers, the dispersions at the VBM and CBM are in agreement with the previous theoretical studies.[12,59] In the literature, there are no reported experimental bandgap values for monolayers except for the single-layer BlueP on Au(111) substrates, i.e., 1.10 eV,[13] which is smaller than its predicted value. Analysis of PDOS (see Fig. S2 in the supplementary material) further reveals that the VBM of MXene monolayers is mainly contributed by the C-p state, while the CBMs are dominated by Sc-d, O-p, and Sc-d states in Sc_2CO_2, $Sc_2C(OH)_2$, and Sc_2CF_2, respectively. We further calculated the ionization potential (I), the electron affinity (χ), and the work function (Φ) of each monolayer as defined below. Once the electrostatic potential level of vacuum (E_{vac}) is determined, these properties can be obtained by comparing energy levels of VBM (E_{VBM}), CBM (E_{CBM}), and Fermi (E_F) with the vacuum level (E_{vac}), i.e., $I = E_{vac} - E_{VBM}$, $\chi = E_{vac} - E_{CBM}$, and $\Phi = E_{vac} - E_F$. The electrostatic potential plot of all monolayers is shown in Fig. S3 of the supplementary material. As listed in Table S1 of the supplementary material, the trends of I, χ, and Φ of BlueP and Sc_2CX_2 monolayers suggest a typical type-II band alignment in BlueP/Sc_2CX_2 heterostructures.

The interlayer lattice mismatch between BlueP and considered MXenes [i.e., Sc_2CO_2, Sc_2CF_2, and $Sc_2C(OH)_2$] is −3.45%, +1.23%, and 0%, respectively, which are in an acceptable range and accessible in the experimental synthesis of BlueP/Sc_2CX_2 heterostructures. The negative (positive) sign represents a small (large) lattice constant of Sc_2CX_2 MXenes with respect to BlueP in a 1 × 1 × 1 supercell. For these systems, six selective stacking configurations with special rotation angles (i.e., 0°, 60°, 120°, 180°, 240°, and 300°) of BlueP with respect to the Sc_2CX_2 layer were explored. The

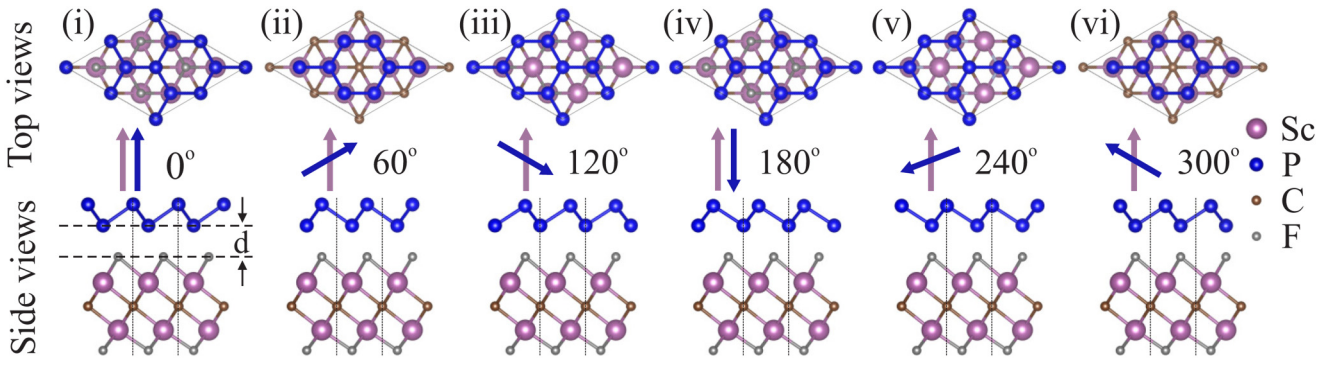

FIG. 1. Top and side views of BlueP/Sc_2CF_2 heterostructures with different stacking configurations in terms of rotation 60° angles of the BlueP monolayer with respect to Sc_2CF_2 (see text for details). The vertical solid line indicates the range of the unit cell. The optimized interlayer distance is indicated by *d* and tabulated in Table I.

simulated structures of the BlueP/Sc_2CF_2 heterostructures are presented in Fig. 1. The stacking patterns of other two heterostructures [BlueP/Sc_2CO_2 and BlueP/$Sc_2C(OH)_2$] are similar and are, therefore, not displayed in the figure. All these configuration were subjected to geometrical optimization. To compare the relative stability of different configurations of the heterostructures, the interface binding energies (E_b) were calculated by

$$E_b = E_{(BlueP/Sc_2CX_2)} - E_{(BlueP)} - E_{(Sc_2CX_2)}, \quad (1)$$

where $E_{(BlueP/Sc_2CX_2)}$, $E_{(BlueP)}$, and $E_{(Sc_2CX_2)}$ represent the total energies of BlueP/Sc_2CX_2 heterostructure, BlueP, and Sc_2CX_2 monolayers fixed in the corresponding heterostructure lattice, respectively. According to the definition, a negative value of E_b suggests that a given BlueP/Sc_2CX_2 interface is stable. The lower absolute value of E_b indicates stronger interactions between the BlueP and Sc_2CX_2 monolayers. The stacking with the large binding energy is referred to be the most favorable one. Binding energies along with an equilibrium interlayer distance (d) are illustrated in Table I. The large binding energies and reasonable (smaller than 3 Å) interlayer distance suggest that patterns (i), (ii), and (v) in BlueP/Sc_2CO_2, BlueP/Sc_2CF_2, and BlueP/$Sc_2C(OH)_2$ are more favorable, respectively. For the BlueP/Sc_2CO_2 heterostructure, other possible patterns (i.e., by placing Sc_2CO_2 MXene on the top BlueP) were also considered but were found less stable than pattern (i). The smaller interlayer distances in BlueP/Sc_2CO_2 and BlueP/$Sc_2C(OH)_2$ when compared to BlueP/Sc_2CF_2 indicate comparably stronger interlayer interactions in the former systems. The calculated binding energies per unit cell for the considered systems are comparable with BlueP/Zr_2CO_2 (−0.235 eV) and BlueP/Hf_2CO_2 (−0.229 eV) and TMDCs/Sc_2CF_2 (−0.268 eV to −0.313 eV) and vdW heterostructures.[60,57]

To further ensure the dynamic stability of patterns (i) BlueP/Sc_2CO_2, (ii) BlueP/Sc_2CF_2, and (v) BlueP/$Sc_2C(OH)_2$, we have performed phonon spectra calculations; see Fig. 2. One can see that phonon spectra exhibit no imaginary frequency, confirming the dynamic stability of both monolayers and heterostructures. It is worth mentioning that the ZA phonon branch in the phonon band structures of the Sc_2CO_2 monolayer and the BlueP/Sc_2CO_2 heterostructure, which corresponds to the out-of-plane vibrations (also called the flexural mode or bending mode), exhibits a U-shaped small imaginary frequency near the Γ point of the Brillouin zone.[77] This U-shaped feature does not indicate the lattice instability but indicates the flexural acoustic mode commonly present in 2D systems.[78–80] Three low frequency optical vibration modes (highlighted with red color) indicate small interlayer coupling in the heterostructures. Similar low frequency optical vibration modes have been observed experimentally in MoS_2/WSe_2 and $MoSe_2/MoS_2$ heterostructures[81] and in other theoretical investigations of vdW heterostructures, i.e., MoS_2/WSe_2, $WS_2/MoSe_2$, $MoSe_2/Zr_2CO_2$, WSe_2/Zr_2CF_2, and SiC-MX_2 (M = Mo, W and X = S, Se) heterostructures.[56,58,82] Therefore, stacking patterns (i), (ii), and (v) are the stable structures with vdW interactions and, hence, are considered in the following.

All the heterostructures retain their semiconducting characteristics well and exhibit indirect bandgaps; see Figs. 3(a)–3(c). The

TABLE I. Binding energy per unit cell (E_b, eV) and the interlayer distance (d, Å) of BlueP/Sc_2CX_2 (X = O, F, and OH) heterostructures for six configurations (patterns i–vi). The bold values represent the largest binding energy among different stackings.

Configuration		BlueP/Sc_2CO_2	BlueP/Sc_2CF_2	BlueP/$Sc_2C(OH)_2$
(i)	E_b	**−0.1894**	−0.1151	−0.2749
	d	2.720	2.759	2.236
(ii)	E_b	−0.1851	**−0.1155**	−0.2711
	d	2.703	2.813	2.211
(iii)	E_b	−0.0850	−0.1018	−0.2665
	d	3.522	2.911	2.256
(iv)	E_b	−0.0864	−0.1016	−0.2685
	d	3.384	2.894	2.265
(v)	E_b	−0.1355	−0.0651	**−0.2888**
	d	2.852	3.475	2.433
(vi)	E_b	−0.1378	−0.0652	−0.2877
	d	2.844	3.487	2.436

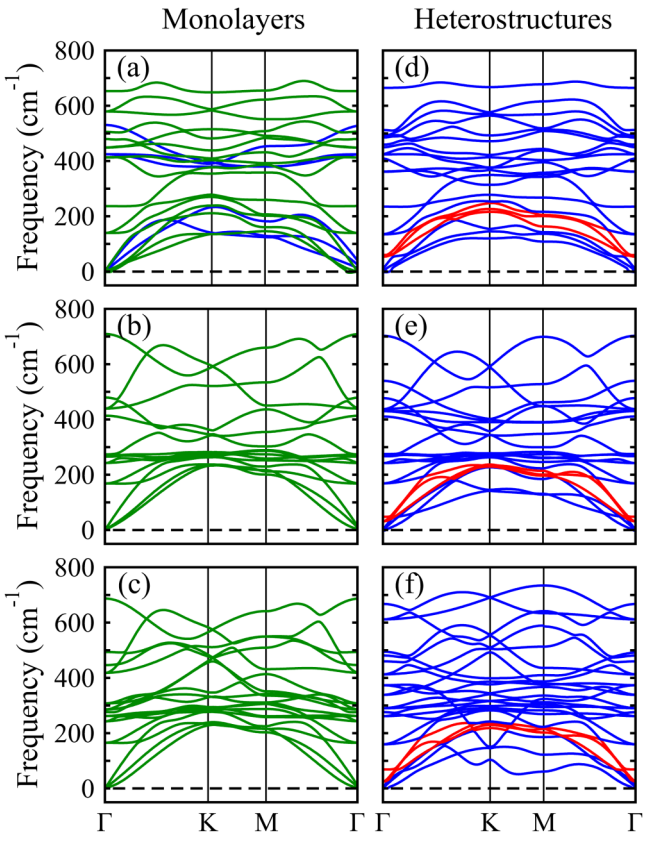

FIG. 2. Phonon dispersion spectra. Left column: blue and green lines represent BlueP and Sc_2CX_2 (X = O, F, and OH) monolayers, respectively: (a) BlueP and Sc_2CO_2, (b) Sc_2CF_2, and (c) $Sc_2C(OH)_2$. Right column: red lines represent low optical modes in (d) BlueP/Sc_2CO_2, (e) BlueP/Sc_2CF_2, and (f) BlueP/$Sc_2C(OH)_2$ heterostructures.

CBMs of the heterostructures are contributed by the BlueP monolayer and thus lie along the M–Γ line, while the VBM is contributed by Sc_2CX_2 and thus is located at the Γ point. Consequently, the bandgaps are significantly reduced, i.e., the bandgaps of BlueP/Sc_2CO_2 and BlueP/$Sc_2C(OH)_2$ are reduced from those of BlueP (2.615 eV), Sc_2CO_2 (2.604 eV), and $Sc_2C(OH)_2$ (0.589 eV) monolayers to 0.218 eV and 0.1504 eV, respectively. In the case of BlueP/Sc_2CF_2, the bandgap is almost identical to that of the Sc_2CF_2 (1.529 eV vs 1.573 eV) monolayer. The large reduction in the bandgap of BlueP/Sc_2CO_2 is due to a large mismatch between corresponding monolayers, as the monolayers are subjected to strains, i.e., the BlueP (Sc_2CO_2) layer is under tension (compression). Modifications in the band structures of heterostructures compared to their parent monolayers reveal significant potential for bandgap engineering by stacking and applying external moderate strain.

The band alignment between the BlueP and Sc_2CX_2 layers is depicted in Fig. 3(d). Clearly, it turns out that the VBM (CBM) of the BlueP layer is lower than that of the Sc_2CX_2 layer, resulting in confinement of holes in the Sc_2CX_2 layers and electrons in BlueP layers. Such type of band alignment is called type-II band alignment. The resemblance of CBMs and VBMs of heterostructures, respectively, with CBM and VBM of BlueP and Sc_2CX_2 pristine monolayers signifies the creation of type-II band alignment. Hence, the BlueP/Sc_2CX_2 heterostructures are type-II (staggered) bandgap semiconductors. Because of electron-hole confinement in different layers, it allows larger offsets on one side.[83] Thus, the BlueP/Sc_2CX_2 vdW heterostructures are promising for applications in unipolar electronic devices.

To reveal the interaction mechanism between BlueP and Sc_2CX_2 layers, the PDOS of BlueP/Sc_2CX_2 heterostructures are also plotted in Figs. 3(a)–3(c). It is clear that the bandgaps from PDOS of BlueP/Sc_2CX_2 heterostructures are consistent with corresponding band structures. The peaks and line patterns of the total DOS (see Fig. S4 in the supplementary material) of heterostructures are similar to those of individual BlueP and Sc_2CX_2 PDOS. The PDOS of the BlueP layer is almost identical in all heterostructures with a little downward movement of states. Furthermore, there is no hybridization between the states (orbitals) of atoms of the BlueP layer with the atoms of Sc_2CX_2 layers, indicating that the layers are combined together with vdW interactions only. Comparatively, BlueP/Sc_2CF_2 is weakly stacked than the other two heterostructures, confirmed by PDOS and its small binding energy.

The electronic states near the Fermi level in the valence band of heterostructures are contributed by the Sc_2CX_2 layer, while the conduction band is mainly dominated by BlueP layer states. The CBMs are due to P-p states of the BlueP layer, whereas the VBMs are due to C-p and Sc-d states of Sc_2CX_2 layers. The weighted band structure analysis (see Fig. S5 in the supplementary material) is in good agreement with PDOS. Hence, the PDOS results and weighted band structures confirm that BlueP/Sc_2CX_2 (X = O, F, OH) heterostructures are type-II semiconductors. The localization of CBMs and VBMs in different layers of BlueP/Sc_2CX_2 heterostructures physically detaches electron-hole pairs, which are obtained without any external effects (i.e., no electric field in our calculations), but still the heterostructures indicate type-II band alignment. This may be due to the intrinsic electric field induced on account of the band bending between the two different monolayers.[84–86] Such intrinsic electric field would drive photogenerated electrons and holes in opposite directions and is thus highly applicable for light harvesting and detection,[50,49] as it provides an effective approach to enhance (reduce) electron-hole separation (recombination) time.

Moreover, the reduction of the bandgap in heterostructures as compared to pristine layers indicates significant interlayer interactions and charge redistribution in these heterostructures. Therefore, to illustrate the specific state of charge transfer, the charge density difference was investigated. The relation is expressed as $\Delta\rho = \rho_{(BlueP/Sc_2CX_2)} - \rho_{(BlueP)} - \rho_{(Sc_2CX_2)}$, where $\rho_{(BlueP/Sc_2CX_2)}$, $\rho_{(BlueP)}$, and $\rho_{(Sc_2CX_2)}$ are the charge densities of BlueP/Sc_2CX_2 heterostructures and pristine monolayers of BlueP and Sc_2CX_2, respectively. As depicted in Figs. 4(a)–4(c), the charge density difference clearly shows that charge depletes mainly from the MXene layer in BlueP/Sc_2CO_2 and BlueP/$Sc_2C(OH)_2$ and from BlueP in BlueP/Sc_2CF_2, while charge accumulates mainly around the interface regions in the former heterostructures.

The plane average charge density difference $\Delta\rho_z$ is estimated to examine the induced charge transfer along the z direction normal to heterostructures, as presented in Figs. 4(d)–4(f). The positive (negative) values indicate charge depletion (accumulation). The $\Delta\rho_z$ confirm that the Sc_2CO_2 [$Sc_2C(OH)_2$] layer donates

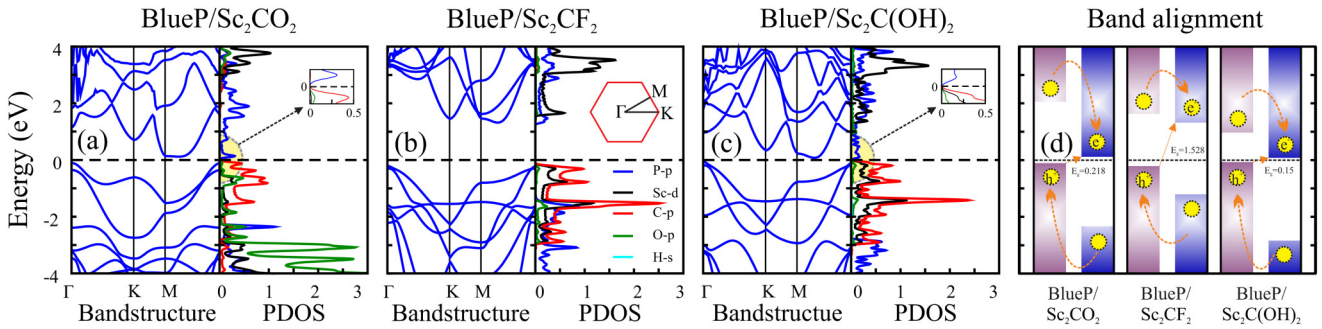

FIG. 3. Band structures (left column) and partial density of states (PDOS) (right column) of heterostructures: (a) BlueP/Sc_2CO_2, (b) BlueP/Sc_2CF_2, and (c) BlueP/$Sc_2C(OH)_2$ given by the hybrid HSE06 functional. (d) The schematic view of the band alignments of BlueP/Sc_2CX_2 (X = O, F, and OH) heterostructures [the blue (purple) color denotes the BlueP (Sc_2CX_2) layer]. The inset in (b) is the hexagonal Brillouin zone of heterostructures with high symmetry k-points.

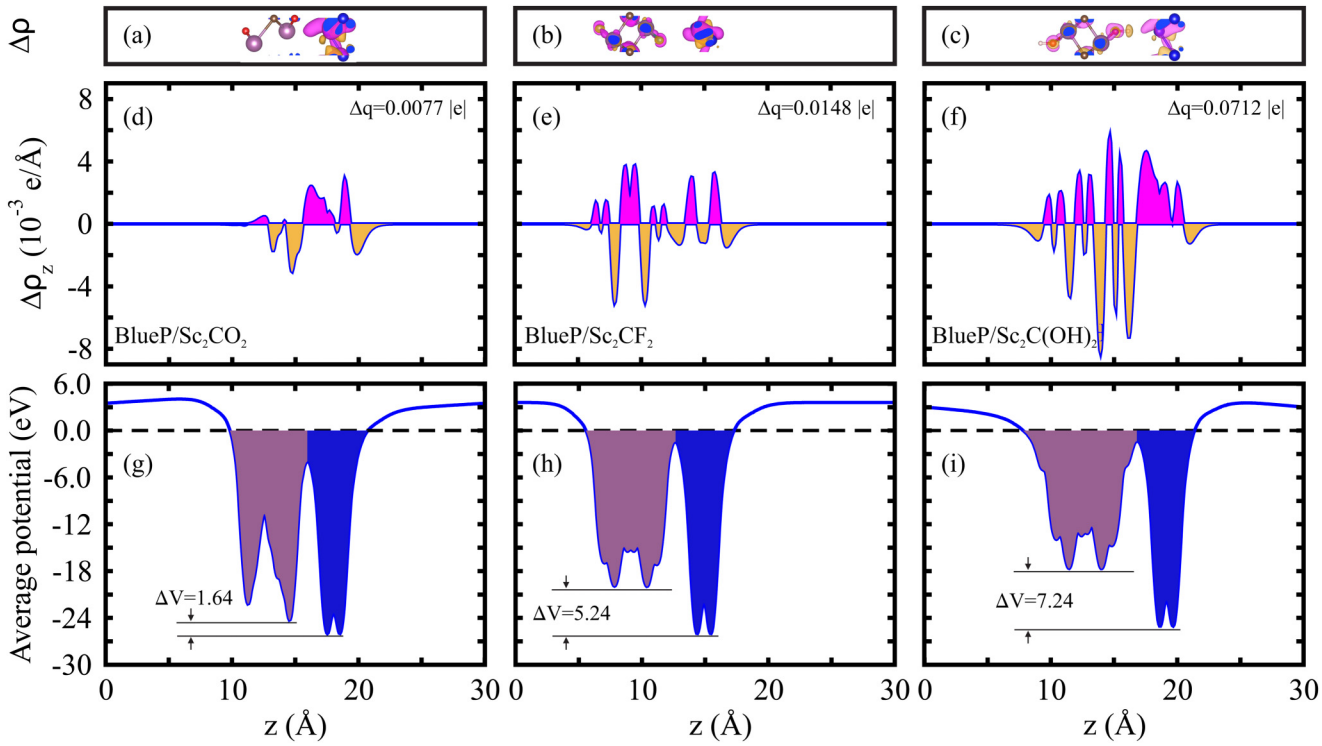

FIG. 4. (a)–(c) The charge density difference ($\Delta\rho$), (d)–(f) plane-averaged electron density difference ($\Delta\rho_z$), and (g)–(i) electrostatic potential along the interface normal of BlueP/Sc_2CO_2, BlueP/Sc_2CF_2, and BlueP/$Sc_2C(OH)_2$ heterostructures, respectively. The orange and magenta areas represent charge depletion and accumulation, respectively (isosurface value: 0.002 e/Å^3).

electron to the BlueP layer in BlueP/Sc_2C_2O (Sc_2CO_2), while Sc_2CF_2 accepts electrons from the BlueP layer in BlueP/Sc_2CF_2, leading to n- and p-type of doping in BlueP, respectively. The charge redistribution in Sc_2CO_2 is more pronounced than the other systems, rationalizing the stronger interfacial interaction. These results suggest that weak interaction does not prevent charge transfer between distinct layers, similar to BlueP/$Mg(OH)_2$, h-BCN/BlueP, BlueP/MS_2 (M = Nb, Ta), SiC(GeC)/MoS_2, and phosphorene/graphene heterostructures.[87–91]

Quantitatively, the total amount of charge transfer between the layers of heterostructure is evaluated by Bader charge analysis. The results show that interlayer charge transfers per unit cell are about 0.0077 $|e|$ (0.0712 $|e|$) from the Sc_2CO_2 [$Sc_2C(OH)_2$] layer to BlueP and 0.0148 $|e|$ from BlueP to Sc_2CF_2 (see Table S2 in the supplementary material). The P atoms of the BlueP layer in the BlueP/Sc_2CO_2 heterostructure accommodate these transferred charges rather than O atoms of the Sc_2CO_2 layer despite higher electronegativity of oxygen when compared to other elements. The reason for such transfer is the compression of the Sc_2CO_2 layer, leading to decreased bond lengths and, hence, increased interlayer charge transfer. The redistribution of charge often leads to an intrinsic electrostatic field across the interface.

The planar average electrostatic potential of the heterostructures is presented in Figs. 4(g)–4(i). The interface region between the layers is separated by different colors (i.e., blue represents the BlueP layer and the Sc_2CX_2 layer is denoted by magenta). The ionization potentials (vacuum energy level) of BlueP/Sc_2CO_2, BlueP/Sc_2CF_2, and BlueP/$Sc_2C(OH)_2$ heterostructures are 5.417 eV (3.516 eV), 5.321 eV (3.612 eV), and 2.771 eV (3.022 eV), respectively, while the electron affinities are presented in Table II. The ionization potentials of the heterostructures follow an order of O > F > OH, similar to that of Sc_2CX_2 monolayers. Furthermore, the potential drops (ΔV) across the BlueP/Sc_2CO_2, BlueP/Sc_2CF_2, and BlueP/$Sc_2C(OH)_2$ heterostructures are found to be 1.64 eV, 5.24 eV, and 7.24 eV, respectively. This built-in electric field across the interface points from one layer to another, consistent with the charge redistribution picture across the interface. Consequently, the carrier dynamics and the excitonic behavior of heterostructures may be significantly influenced, as compared to isolated monolayers, when they are used in the nanoelectric devices.[92,93]

Finally, as mentioned above, efficient interlayer charge transfer may influence optical absorption of the heterostructures with respect to pristine monolayers. Therefore, we analyzed the imaginary part of the dielectric function [$\varepsilon_2(\omega)$] of monolayers and heterostructures. The absorption spectra of $\varepsilon_2(\omega)$ depicted in Figs. 5(a)–5(d) demonstrate that the optical transitions are dominated by excitons. The BlueP and Sc_2CO_2 monolayers have a first excitonic peak at 2.77 eV and 2.94 eV, respectively, within the visible

TABLE II. Optimized lattice constant (a, Å), bond length (Sc-C, Sc-X, and P-P, Å), the out-of-plane height (H-P, Å) of the BlueP layer, bandgap (E_g, eV), work function (Φ, eV), ionization potential (I, eV), and electron affinity (χ, eV) of BlueP/Sc_2CX_2 (X = O, F, and OH) heterostructures. (E_g, Φ, I, and χ are obtained using the HSE06 hybrid functional.)

Heterostructures	BlueP/Sc_2CO_2	BlueP/Sc_2CF_2	BlueP/$Sc_2C(OH)_2$
a	3.390	3.266	3.300
Sc-C	2.207	2.271	2.310
Sc-X	2.048	2.188	2.219
P-P	2.286	2.253	2.252
H-P	1.181	1.233	1.202
E_g	0.2182	1.529	0.1504
Φ	5.312	5.112	2.699
I	5.417	5.321	2.771
χ	5.199	3.791	2.620

light region (<3.0 eV), whereas for Sc_2CF_2 and $Sc_2C(OH)_2$, the peaks are at 2.00 eV and 0.1 eV. The red shift in monolayers from BlueP to Sc_2CO_2 to Sc_2CF_2 to $Sc_2C(OH)_2$ is due to their decreasing bandgaps. The optical transitions of Sc_2CX_2 monolayers are consistent with the previous studies using PBE and HSE06 functionals.[35] Small differences in peaks positions of the BlueP monolayer compared to Ref. 94 are because small number k-points were adopted in this study due to the large computational cost. The BlueP and Sc_2CO_2 monolayers show large light absorption in the ultraviolet (UV) region, and the largest strength of absorption appeared at 4 eV to 4.5 eV, respectively. Contrastingly, the Sc_2CF_2 and $Sc_2C(OH)_2$ monolayers have apparent absorption in the visible region (from 1.6 eV to 3.0 eV) of light, indicating the harvest of the major portion of visible light.

Stacking BlueP with Sc_2CO_2 and $Sc_2C(OH)_2$ in terms of vdW interaction [i.e., BlueP/Sc_2CO_2 and BlueP/$Sc_2C(OH)_2$] demonstrate significant red shifts and promotion of the oscillator strength peak from 4 eV to 5 eV and from 1 eV to 2 eV, respectively. In contrast, the absorption peaks of the BlueP/Sc_2CF_2 are almost similar to that of the Sc_2CF_2 monolayer from 2 eV to 2.55 eV and the BlueP monolayer from 4 eV to 4.5 eV with a little blue shift, confirming a small interlayer coupling in BlueP/Sc_2CF_2 as compared to other two heterostructures. This behavior is related to the aforementioned results that the interlayer charge transfer can influence the optical transition. Noticeably, the decrease of the bandgap results in a red shift of the absorption peaks. As a result, the narrower bandgaps in BlueP/Sc_2CO_2 and BlueP/$Sc_2C(OH)_2$ heterostructures possess higher absorption efficiency in the visible light range relative to their corresponding wide bandgaps of the monolayer systems. The enhancement and red shift to the visible light region of the absorption spectra indicate that BlueP/Sc_2CX_2 heterostructures could be a potential candidate for light driven photocatalysis and other photoelectronic processes.

Light absorption efficiency is an important aspect to evaluate the device's performance in the presence of sunlight. Therefore, we calculated the absorption efficiencies for all considered 2D materials (predicted MXenes and BlueP) as shown in Figs. 6(a)–6(d). The Sc_2CF_2 monolayer has a high absorption efficiency, more than 70%

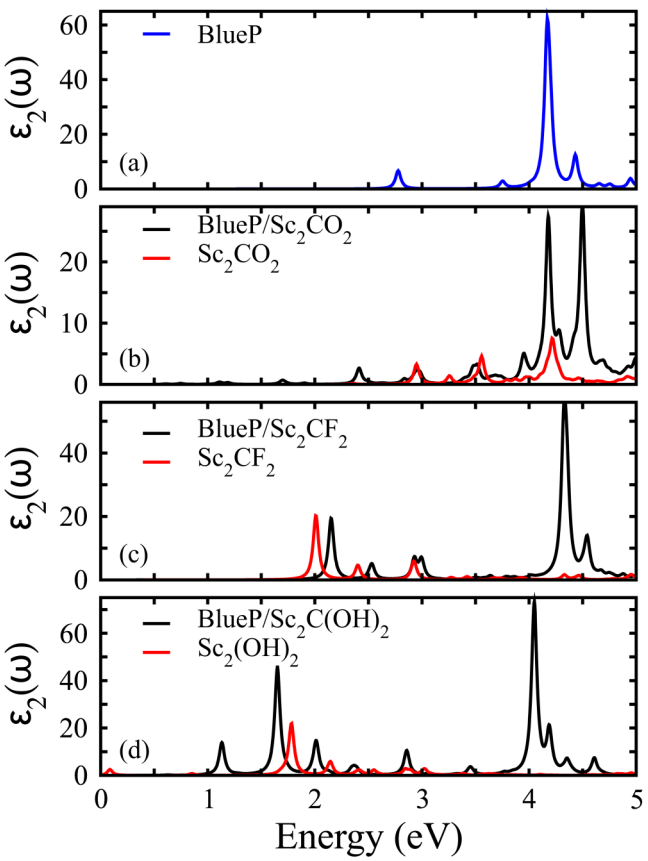

FIG. 5. Imaginary part of the dielectric function $\varepsilon_2(\omega)$ of heterostructures along with monolayers. (a) BlueP (blue), (b) Sc_2CO_2 and BlueP/Sc_2CO_2, (c) Sc_2CF_2 and BlueP/Sc_2CF_2, and (d) $Sc_2C(OH)_2$ and BlueP/$Sc_2C(OH)_2$. The blue and red and black lines represent BlueP and Sc_2CX_2 (X = O, F, and OH) monolayers and heterostructures, respectively.

in the wavelength range of 300–700 nm (ultraviolet and visible range). For the $Sc_2C(OH)_2$ monolayer, the absorption efficiency is in the range of 60%–90% (in the wavelength range below 750 nm), while an abrupt decrease above 750 nm can be observed. In cases of Sc_2CO_2 and BlueP monolayers, the absorption efficiency lies in a narrow wavelength window (below 470 nm), covering the ultraviolet region of light. The absorption efficiencies are considerably increased in their vdW heterostructures, particularly in the visible range of light spectrum. From Fig. 6(d), BlueP/$Sc_2C(OH)_2$ heterostructure shows absorption efficiency in a very wide range of wavelengths (~1200 nm) with the absorption efficiency above 80%, which covers the entire light spectrum (visible, infrared, and ultraviolet). The absorption efficiency of the BlueP/Sc_2CO_2 heterostructure is almost identical to the $Sc_2C(OH)_2$ monolayer. Similar to the Sc_2CF_2 monolayer, the BlueP/Sc_2CF_2 heterostructures show very high absorption efficiency (above 70%) in the ultraviolet and visible range. These results suggest that the BlueP/Sc_2CX_2 heterostructures show excellent absorption efficiencies in the entire spectrum of light reaching the surface of the earth. Recently, for Janus (WSeTe, MoSTe,

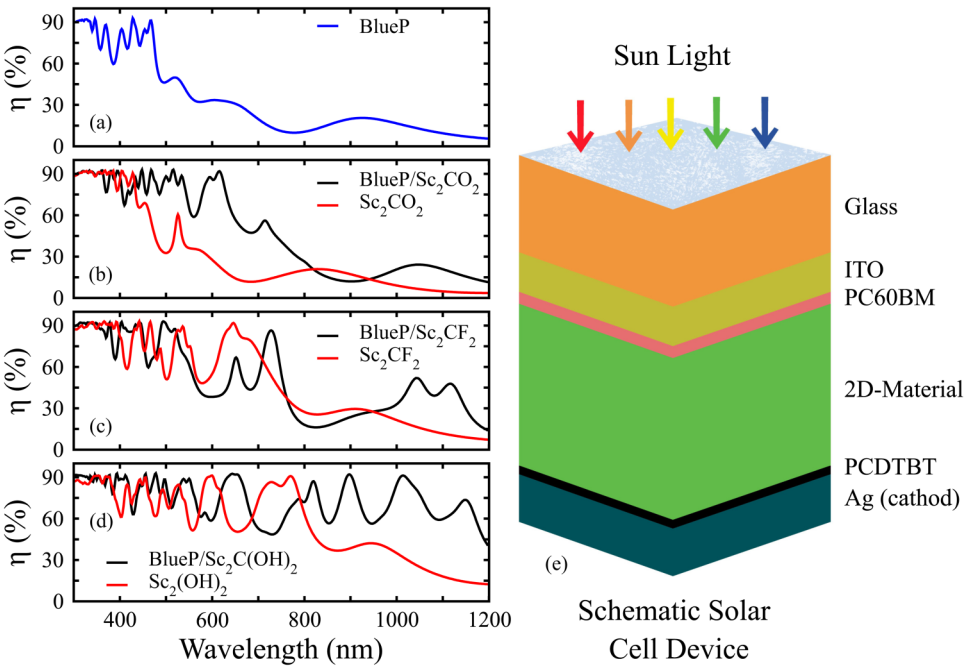

FIG. 6. (a)–(d) Solar cell device absorption efficiencies for 2D monolayers and heterostructures. (e) A schematic solar cell device used for absorption efficiency calculations in this study.

and WSTe monolayers) materials, similar absorption efficiencies (80%–90%) in the visible, infrared, and ultraviolet spectrum ranges are predicted.[95] Besides BlueP/Sc_2CF_2, we expect a very strong power conversion efficiency in the case of BlueP/$Sc_2C(OH)_2$ for photovoltaic applications.

IV. CONCLUSION

In summary, using HSE06 hybrid functional with vdW corrections, we systematically investigated the electronic structures and optical properties of BlueP/Sc_2CX_2 (X = O, F, OH) vdW heterostructures and their corresponding monolayers. The negative binding energies and the absence of imaginary frequencies in phonon dispersion spectra suggest that the considered three BlueP/Sc_2CX_2 heterostructures and corresponding monolayers are stable. The band structures and PDOS reveal that all heterostructures are indirect semiconductors with type-II band alignment. Infinitesimal charge transfer across the interfaces of BlueP and MXenes layers still produces electrostatic fields, which facilitates the separation of electrons and holes. In the visible range, optical absorption is improved, inducing red shifts in BlueP/Sc_2CO_2 and BlueP/$Sc_2C(OH)_2$ and a blue shift in BlueP/Sc_2CF_2. Furthermore, the excitonic transitions are modified with respect to the parent monolayers. These findings reveal that BlueP/Sc_2CO_2, BlueP/Sc_2CF_2, and BlueP/$Sc_2C(OH)_2$ heterostructures are promising candidates for novel electronic/optical device applications. Particularly, the BlueP/$Sc_2C(OH)_2$ heterostructure shows an excellent absorption efficiency of 80% (1200 nm) in the entire spectrum of light reaching the surface of the earth. Hence, in addition to BlueP/Sc_2CF_2, we are expecting a very strong power conversion efficiency of BlueP/$Sc_2C(OH)_2$ for photovoltaic applications.

SUPPLEMENTARY MATERIAL

The electronic structure of BlueP, Sc_2CX_2 (X = O, F, OH) monolayers, and BlueP/Sc_2CX_2 van der Waals heterostructures are presented in the supplementary material.

ACKNOWLEDGMENTS

The authors acknowledge financial support from the Higher Education Commission of Pakistan (HEC) (Project No. 20-3959/NRPU/R&D/HEC2014/234) and HEC's IRSIP program.

REFERENCES

[1]K. S. Novoselov, A. K. Geim, S. V. Morozov, D. Jiang, Y. Zhang, S. V. Dubonos, I. V. Grigorieva, and A. A. Firsov, Science **306**, 666 (2004).
[2]B. Aufray, A. Kara, S. Vizzini, H. Oughaddou, C. Léandri, B. Ealet, and G. Le Lay, Appl. Phys. Lett. **96**, 183102 (2010).
[3]Q.-X. Pei, Z.-D. Sha, Y.-Y. Zhang, and Y.-W. Zhang, J. Appl. Phys. **115**, 023519 (2014).
[4]X. Wu, J. Dai, Y. Zhao, Z. Zhuo, J. Yang, and X. C. Zeng, ACS Nano **6**, 7443 (2012).
[5]Y. Gao, X. Zhang, Y. Jing, and M. Hu, Nanoscale **7**, 7143 (2015).
[6]R. Ma and T. Sasaki, Adv. Mater. **22**, 5082 (2010).
[7]H. Liu, A. T. Neal, Z. Zhu, Z. Luo, X. Xu, D. Tománek, and P. D. Ye, ACS Nano **8**, 4033 (2014).
[8]K. S. Novoselov, V. I. Falko, L. Colombo, P. R. Gellert, M. G. Schwab, and K. Kim, Nature **490**, 192 (2012).
[9]W. Yuan and G. Shi, J. Mater. Chem. A **1**, 10078 (2013).
[10]M. Yu, W. Yuan, C. Li, J.-D. Hong, and G. Shi, J. Mater. Chem. A **2**, 7360 (2014).
[11]L. Kou, C. Chen, and S. C. Smith, J. Phys. Chem. Lett. **6**, 2794 (2015).
[12]Z. Zhu and D. Tománek, Phys. Rev. Lett. **112**, 176802 (2014).

[13]J. L. Zhang, S. Zhao, C. Han, Z. Wang, S. Zhong, S. Sun, R. Guo, X. Zhou, C. D. Gu, K. D. Yuan, Z. Li, and W. Chen, Nano Lett. **16**, 4903 (2016).
[14]J. Zeng, P. Cui, and Z. Zhang, Phys. Rev. Lett. **118**, 046101 (2017).
[15]J. Qiao, X. Kong, Z.-H. Hu, F. Yang, and W. Ji, Nat. Commun. **5**, 4475 (2014).
[16]V. Tran, R. Soklaski, Y. Liang, and L. Yang, Phys. Rev. B **89**, 235319 (2014).
[17]H. O. Churchill and J.-H. Pablo, Nat. Nanotechnol. **9**, 330 (2014).
[18]S. P. Koenig, R. A. Doganov, H. Schmidt, A. H. C. Neto, and B. Ozyilmaz, Appl. Phys. Lett. **104**, 103106 (2014).
[19]S. Das, W. Zhang, M. Demarteau, A. Hoffmann, M. Dubey, and A. Roelofs, Nano Lett. **14**, 5733 (2014).
[20]M. Naguib, M. Kurtoglu, V. Presser, J. Lu, J. Niu, M. Heon, L. Hultman, Y. Gogotsi, and M. W. Barsoum, Adv. Mater. **23**, 4248 (2011).
[21]M. Naguib, O. Mashtalir, J. Carle, V. Presser, J. Lu, L. Hultman, Y. Gogotsi, and M. W. Barsoum, ACS Nano **6**, 1322 (2012).
[22]O. Mashtalir, M. Naguib, B. Dyatkin, Y. Gogotsi, and M. W. Barsoum, Mater. Chem. Phys. **139**, 147 (2013).
[23]M. Naguib, J. Halim, J. Lu, K. M. Cook, L. Hultman, Y. Gogotsi, and M. W. Barsoum, J. Am. Chem. Soc. **135**, 15966 (2013).
[24]M. Naguib, V. N. Mochalin, M. W. Barsoum, and Y. Gogotsi, Adv. Mater. **26**, 992–1005 (2013).
[25]M. Pandey and K. S. Thygesen, J. Phys. Chem. C **121**, 13593 (2017).
[26]C. Si, K.-H. Jin, J. Zhou, Z. Sun, and F. Liu, Nano Lett. **16**, 6584 (2016).
[27]C. Si, J. Zhou, and Z. Sun, ACS Appl. Mater. Inter. **7**, 17510 (2015).
[28]Y. Xie, Y. DalÁgnese, M. Yohan, Y. Gogotsi, M. W. Barsoum, H. L. Zhuang, and P. R. C. Kent, ACS Nano **8**, 9606 (2014).
[29]X. Wang, S. Kajiyama, H. Iinuma, E. Hosono, S. Oro, I. Moriguchi, M. Okubo, and A.-S. Yamada, Nat. Commun. **6**, 6544 (2015).
[30]M. Naguib, R. A. Adams, Y. Zhao, D. Zemlyanov, A. Varma, J. Nanda, and V. G. Pol, Chem. Commun. **53**, 6883 (2017).
[31]Z. Guo, L. Zhu, J. Zhou, and Z. Sun, RSC Adv. **5**, 25403 (2015).
[32]F. Shahzad, M. Alhabeb, C. B. Hatter, B. Anasori, S. Man Hong, C. M. Koo, and Y. Gogotsi, Science **353**, 1137 (2016).
[33]Z. Guo, J. Zhou, C. Si, and Z. Sun, Phys. Chem. Chem. Phys. **17**, 15348 (2015).
[34]S. Ma, D. Yuan, Z. Jiao, T. Wang, and X. Dai, J. Phys. Chem. C **121**, 24077 (2017).
[35]K. Xiong, P. Wang, G. Yang, Z. Liu, H. Zhang, S. Jin, and X. Xu, Sci. Rep. **7**, 15095 (2017).
[36]H.-P. Komsa, J. Kotakoski, S. Kurasch, O. Lehtinen, U. Kaiser, and A. V. Krasheninnikov, Phys. Rev. Lett. **109**, 035503 (2012).
[37]B. Amin, T. P. Kaloni, and U. Schwingenschlögl, RSC Adv. **4**, 34561 (2014).
[38]H.-P. Komsa and A. V. Krasheninnikov, Phys. Rev. B **88**, 085318 (2013).
[39]X. Hong, J. Kim, S.-F. Shi, Y. Zhang, C. Jin, Y. Sun, S. Tongay, J. Wu, Y. Zhang, and F. Wang, Nat. Nanotechnol. **9**, 682 (2014).
[40]N. Lu, H. Guo, L. Wang, X. Wu, and X. C. Zeng, Nanoscale **6**, 4566 (2014).
[41]Y. Mogulkoc, M. Modarresi, A. Mogulkoc, and Y. Ciftci, Comput. Mater. Sci. **124**, 23 (2016).
[42]T. Roy, M. Tosun, X. Cao, H. Fang, D.-H. Lien, P. Zhao, Y.-Z. Chen, Y.-L. Chueh, J. Guo, and L. Javey, ACS Nano **9**, 2071 (2015).
[43]L.-S. Oriol, A. L. Esther, K. Volodymyr, F. M. Anna, R. Aleksandra, and K. Andras, ACS Nano **8**, 3042 (2014).
[44]N. Huo, J. Kang, Z. Wei, S.-S. Li, J. Li, and S.-H. Wei, Adv. Funct. Mater. **24**, 7025 (2014).
[45]A. K. Geim and I. V. Grigorieva, Nature **499**, 419 (2013).
[46]K. S. Novoselov, A. Mishchenko, A. Carvalho, and N. A. H. Castro, Science **353**, aac9439 (2016).
[47]Y. Hu, X. Li, A. Lushington, M. Cai, D. Geng, M. N. Banis, R. Li, and X. Sun, ECS J. Solid State Sci. Technol. **2**, 3034 (2013).
[48]B. Simone, K. Daria, and K. Andras, ACS Nano **7**, 3246 (2013).
[49]J. Kang, S. Tongay, J. Zhou, J. Li, and J. Wu, Appl. Phys. Lett. **102**, 012111 (2013).
[50]X.-L. Wei, H. Zhang, G.-C. Guo, X.-B. Li, W.-M. Lau, and L.-M. Liu, J. Mater. Chem. A **2**, 2101 (2014).
[51]Q. Peng, Z. Wang, B. Sa, B. Wu, and Z. Sun, Sci. Rep. **6**, 31994 (2016).
[52]V. O. Özçelik, J. G. Azadani, C. Yang, S. J. Koester, and T. Low, Phys. Rev. B **94**, 035125 (2016).
[53]R. Cheng, D. Li, H. Zhou, C. Wang, A. Yin, S. Jiang, Y. Liu, Y. Chen, Y. Huang, and X. Duan, Nano Lett. **14**, 5590 (2014).
[54]P. Rivera, J. R. Schaibley, A. M. Jones, J. S. Ross, S. Wu, G. Aivazian, P. Klement, K. Seyler, G. Clark, N. J. Ghimire, J. Yan, D. G. Mandrus, W. Yao, and X. Xu, Nat. Commun. **6**, 6242 (2015).
[55]Y. Deng, Z. Luo, N. J. Conrad, H. Liu, Y. Gong, S. Najmaei, P. M. Ajayan, J. Lou, X. Xu, and P. D. Ye, ACS Nano **8**, 8292 (2014).
[56]G. Rehman, S. A. Khan, B. Amin, I. Ahmad, L.-Y. Gan, and M. Maqbool, J. Mater. Chem. C **6**, 2830 (2018).
[57]Z. Ma, Z. Hu, X. Zhao, Q. Tang, D. Wu, Z. Zhou, and L. Zhang, J. Phys. Chem. C **118**, 5593 (2014).
[58]H. U. Din, M. Idrees, G. Rehman, C. V. Nguyen, L.-Y. Gan, I. Ahmad, M. Maqbool, and B. Amin, Phys. Chem. Chem. Phys. **20**, 24168 (2018).
[59]Y. Lee, Y. Hwang, and Y.-C. Chung, ACS Appl. Mater. Int. **7**, 7163 (2015).
[60]Z. Guo, N. Miao, J. Zhou, B. Sa, and Z. Sun, J. Mater. Chem. C **5**, 978 (2017).
[61]Q.-X. Pei, X. Zhang, Z. Ding, Y.-Y. Zhang, and Y.-W. Zhang, Phys. Chem. Chem. Phys. **19**, 17180 (2017).
[62]S. S. Lo, T. Mirkovic, C.-H. Chuang, C. Burda, and G. D. Scholes, Adv. Mater. **23**, 180 (2011).
[63]W. Kohn and L. J. Sham, Phys. Rev. **140**, A1133 (1965).
[64]P. E. Blöchl, Phys. Rev. B **50**, 17953 (1994).
[65]G. Kresse and J. Hafner, Phys. Rev. B **47**, 558 (1993).
[66]J. P. Perdew, K. Burke, and M. Ernzerhof, Phys. Rev. Lett. **77**, 3865 (1996).
[67]S. Grimme, J. Comput. Chem. **27**, 1787 (2006).
[68]S. Baroni, S. de Gironcoli, A. Dal Corso, and P. Giannozzi, Rev. Mod. Phys. **73**, 515 (2001).
[69]A. Togo, F. Oba, and I. Tanaka, Phys. Rev. B **78**, 134106 (2008).
[70]J. Heyd, G. E. Scuseria, and M. Ernzerhof, J. Chem. Phys. **124**, 219906 (2006).
[71]M. Shishkin and G. Kresse, Phys. Rev. B **74**, 035101 (2006).
[72]M. Rohlfing and S. G. Louie, Phys. Rev. Lett. **81**, 2312 (1998).
[73]R. Ali, G.-J. Hou, Z.-G. Zhu, Q.-B. Yan, Q.-R. Zheng, and G. Su, Chem. Mater. **30**, 718 (2018).
[74]R. Ali, G.-J. Hou, Z.-G. Zhu, Q.-B. Yan, Q.-R. Zheng, and G. Su, J. Mater. Chem. A **6**, 9220 (2018).
[75]M. Khazaei, M. Arai, T. Sasaki, C. Y. Chung, N. S. Venkataramanan, M. Estili, Y. Sakka, and Y. Kawazoe, Adv. Funct. Mater. **23**, 2185 (2012).
[76]Y. Ding and Y. Wang, J. Phys. Chem. C **119**, 10610 (2015).
[77]J.-W. Jiang, B.-S. Wang, J.-S. Wang, and H. S. Park, J. Phys. Condens. Matter **27**, 083001 (2015).
[78]S. Singh and A. H. Romero, Phys. Rev. B **95**, 165444 (2017).
[79]M. Idrees, H. U. Din, S. A. Khan, I. Ahmad, L.-Y. Gan, C. V. Nguyen, and B. Amin, J. Appl. Phys. **125**, 094301 (2019).
[80]H. Zheng, X.-B. Li, N.-K. Chen, S.-Y. Xie, W. Q. Tian, Y. Chen, H. Xia, S. B. Zhang, and H.-B. Sun, Phys. Rev. B **92**, 115307 (2015).
[81]C. H. Lui, Z. Ye, C. Ji, K.-C. Chiu, C.-T. Chou, T. I. Andersen, C. Means-Shively, H. Anderson, J.-M. Wu, T. Kidd, Y.-H. Lee, and R. He, Phys. Rev. B **91**, 165403 (2015).
[82]B. Amin, T. P. Kaloni, G. Schreckenbach, and M. Freund, Appl. Phys. Lett. **108**, 063105 (2016).
[83]V. O. Özçelik, J. G. Azadani, C. Yang, S. J. Koester, and T. Low, Phys. Rev. B **94**, 035125 (2016).
[84]T. P. Kaloni, G. Schreckenbach, and M. Freund, J. Phys. Chem. C **118**, 23361 (2014).
[85]T. P. Kaloni, G. Schreckenbach, and M. Freund, J. Phys. Chem. C **119**, 3979 (2015).
[86]T. P. Kaloni, M. Modarresi, M. Tahir, M. R. Roknabadi, G. Schreckenbach, and M. Freund, J. Phys. Chem. C **119**, 11896 (2015).

[87]B.-J. Wang, X.-H. Li, X.-L. Cai, W.-Y. Yu, L.-W. Zhang, R.-Q Zhao, and S.-H. Ke, J. Phys. Chem. C **122**, 7075 (2018).
[88]T. Kaewmaraya, P. Srepusharawoot, T. Hussian, and V. Amornkitbamrung, Chem. Phys. Chem. **19**, 612 (2018).
[89]Q. Peng, Z. Wang, B. Sa, B. Wu, and Z. Sun, ACS Appl. Mater. Int. **8**, 13449 (2016).
[90]Y. C. Rao, S. Yu, and X.-M. Duan, Phys. Chem. Chem. Phys. **19**, 17250 (2017).
[91]Y. Cai, G. Zhang, and Y. W. Zhang, J. Phys. Chem. C **119**, 13929 (2015).
[92]Y. Cai, Q. Ke, G. Zhang, and Y. W. Zhang, J. Phys. Chem. C **119**, 3102 (2015).
[93]J. Liu, J. Phys. Chem. C **119**, 28417 (2015).
[94]C. E. P. Villegas, A. S. Rodin, A. Carvalho, and A. R. Rocha, Phys. Chem. Chem. Phys. **18**, 27829 (2016).
[95]M. Idrees, H. U. Din, R. Ali, G. Rehman, T. Hussian, C Nguyen, I. Ahmad, and B. Amin, Phys. Chem. Chem. Phys. **21**, 18612 (2019).